

Supersandwich Cytosensor for Selective and Ultrasensitive Detection of Cancer Cells Using Aptamer-DNA Concatamer-Quantum Dots Probes

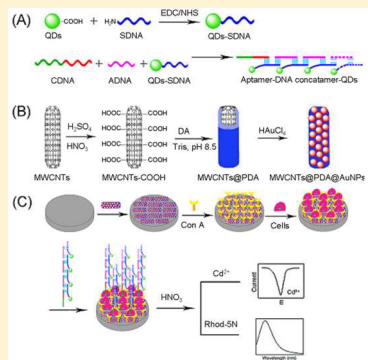
Hongying Liu,[†] Shouming Xu,^{†,‡} Zhimei He,[†] Anping Deng,^{*,‡} and Jun-Jie Zhu^{*,†}

[†]State Key Lab of Analytical Chemistry for Life Science, School of Chemistry & Chemical Engineering, Nanjing University, Nanjing 210093, China

[‡]The Key Lab of Health Chemistry & Molecular Diagnosis of Suzhou, College of Chemistry, Chemical Engineering & Materials Science, Soochow University, Suzhou 215123, China

S Supporting Information

ABSTRACT: In this work, a signal amplification supersandwich strategy was developed for highly selective and sensitive detection of cancer cells using aptamer-DNA concatamer-quantum dots (QDs) probes. First of all, electrode materials denoted as MWCNTs@PDA@AuNPs were fabricated by multiwall carbon nanotubes (MWCNTs), gold nanoparticles (AuNPs), and polydopamine (PDA) using a layer-by-layer technique. Then, the prepared bases as matrices were applied to bind concanavalin A (Con A), resulting in high stability, bioactivity, and capability for cell capture. Meanwhile, aptamer-DNA concatamer-QDs were designed via DNA hybridization followed by covalent assembling, which incorporated the specific recognition of the aptamer with the signal amplification of the DNA concatamer and QDs. With aptamer-DNA concatamer-QDs as recognizing probes, the model cancer cells (CCRF-CEM cells) were detected using a MWCNTs@PDA@AuNPs modified electrode with trapped Con A by means of fluorescence and electrochemical methods. The proposed supersandwich cytosensor showed high sensitivity with the detection limit of 50 cells mL⁻¹. More importantly, it could distinguish cancer cells from normal cells, which indicated the promising applications of our method in clinical diagnosis and treatment of cancers.



Cancer is considered a worldwide mortal sickness and has become a major public concern. Identification and detection of cancer cells can provide an easy and effective way to monitor the progressions of diseases and their relevant biological processes.^{1–3} Thus, it is highly desirable to develop rapid, sensitive, and specific methods to diagnose cancers. Currently, typical methods have been applied in the field of cancer research including immunohistochemistry, polymerase chain reaction, and flow cytometry.^{4–6} However, the selectivity of these methods is not satisfactory. To overcome this problem, aptamers are chosen as molecular probes for specific recognition of cancer cells due to their salient properties, such as high affinity and specificity, ease of chemical modification, good stability, and low immunogenicity.^{7–9}

With the remarkable development of nanotechnology, nanomaterials have been extensively used to enhance the sensitivity of cytosensors.^{10–12} Among them, QDs attract more and more interest because of their unique properties such as high fluorescence efficiency and versatility in surface modification.^{13–15} In addition, QDs are well recognized as electroactive species for signal amplification.^{16,17} Besides that, metal-sensitive dyes such as Rhod-5N can be turned on by Cd²⁺,¹⁸ which promote the intensity of signals several hundred times.^{19–21} On the basis of their fullerene-related structures, multiwall carbon nanotubes (MWCNTs) have many advantages (i.e., stability and biocompatibility) in the construction of

biosensors.^{22,23} Meanwhile, gold nanoparticles (AuNPs) possess the merits of high surface reactivity, good solubility, and excellent bioactivity.^{24,25} Therefore, a technique has emerged to integrate MWCNTs with AuNPs. Recently, dopamine (DA) self-polymerization has been a powerful approach for multifunctional coatings, which forms an adhesion layer to immobilize biomolecules.^{26,27} Inspired by the fascinating molecule (DA), MWCNTs are easily coated with the reactive polydopamine (PDA), followed by the deposition of AuNPs to form MWCNTs@PDA@AuNPs composites. The composites as matrices are further applied in the fabrication of cytosensors.

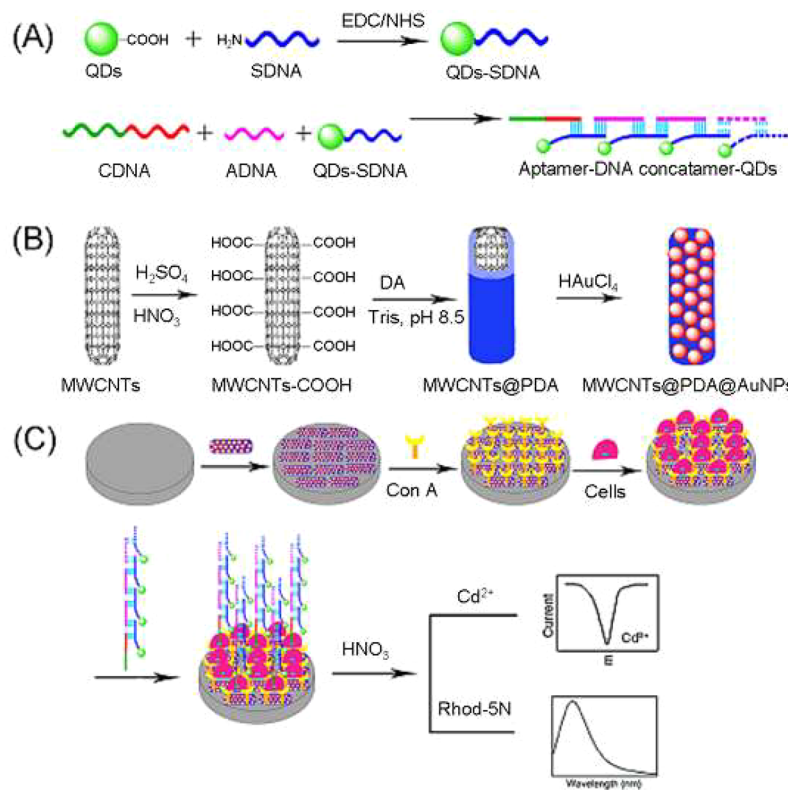
A conventional sandwich model has been widely applied in the determination of DNA, proteins, cells, and small molecules.^{28–31} However, it has an intrinsic limitation on sensitivity, because each probe captures only one target molecule. To solve this problem, Heeger et al. proposed a “supersandwich” model.³² In this case, a signal probe hybridized to complementary regions on each of two target molecules to create long DNA concatamers with multiple target molecules and signal probes, which obtained a higher signal than the

Received: January 10, 2013

Accepted: February 18, 2013

Published: February 18, 2013

Scheme 1. Procedures for the Fabrication of Aptamer-DNA Concatamer-QDs (A), MWCNTs@PDA@AuNPs Composites (B), and Supersandwich Cytosensor (C)



conventional sandwich assay. However, the detection limit of this strategy was also limited since numerous targets participated in the construction of the DNA concatamer. To further improve the sensitivity, some biosensors have been developed by introducing an auxiliary DNA that hybridizes to different regions of a signal probe and self-assembly with signal probes to form long DNA concatamers.^{33–36} Combining the signal amplification of both the DNA concatamer linked with auxiliary DNA and QDs with Cd^{2+} -sensitized fluorescence or electrochemical analysis, dual-signal amplification probes are designed in the fabrication of supersandwich cytosensors.

Herein, we developed a novel approach for selective determination of cancer cells by combining specificity of the aptamer with signal amplification of the DNA concatamer and QDs. The aptamer-DNA concatamer-QDs were prepared at first as shown in Scheme 1A. Then, MWCNTs@PDA@AuNPs composites (Scheme 1B) were assembled to the electrode. The composites were used as matrices for immobilization of concanavalin A (Con A) and played a critical role in signal amplification. As a proof-of-concept, CCRF-CEM cancer cells were selected as model samples to demonstrate the feasibility of the supersandwich strategy. Finally, with aptamer-DNA concatamer-QDs as probes, a dual-channel route with fluorescence and electrochemical method were carried out (Scheme 1C). The proposed strategy exhibited good sensitivity and selectivity, indicating wide applications on aspects of cancer progression studies.

■ EXPERIMENTAL SECTION

Chemicals and Materials. Con A, 1-(3-(dimethylamino)-propyl)-3-ethylcarbodiimide hydrochloride (EDC), N-hydroxysulfosuccinimide (NHS), and tris(2-carboxyethyl) phosphine

hydrochloride (TCEP) were purchased from Sigma-Aldrich. 3-Mercaptopropionic acid (MPA, 99%), sodium borohydride (98%), and tris-(hydroxymethyl) aminomethane (Tris) were purchased from Nanjing Chemical Reagents Factory (Nanjing, China). Reagents for polyacrylamide gel electrophoresis and all DNA sequences were obtained from Sangon Biotechnology Co., Ltd. (Shanghai, China). Cell culture reagents were purchased from Nanjing KenGen Biotech Co., Ltd. (Nanjing, China). All other chemicals involved in this work were analytical-grade. All solutions were freshly prepared using ultrapure water ($\geq 18 \text{ M}\Omega$, Millipore).

DNA sequences are as follows. Capture DNA (CDNA1): 5'-ATC TAA CTG CTG CGC CGC CGG GAA AAT ACT GTA CGG TTA GA TTT TTT TTT TTT CGACA TATCG TGCCA ATTAG-3'. Signal DNA (SDNA): 5'-NH₂-TGACA TTTGC TCGAT TCCTA TACGA GTGGC TATCT TTCGT CTAAT TGGCA CGATA TGTCG-3'. Auxiliary DNA (ADNA): 5'-ACGAA AGATA GCCAC TCGTA TTCAT CACTG GACCG ATACG CGACA TATCG TGCCA ATTAG-3'. Control DNA (CDNA2): 5'-ATC TAA CTG CTG CGC CGC CGG GAA AAT ACT GTA CGG TTA GA TTT TTT TTT TTT CGACA TATCG TGCCA ATTAG-3NH₂'

Apparatus and Characterization. UV-vis absorbance and fluorescence measurements were recorded on a UV-3600 spectrophotometer and an RF-5301PC (Shimadzu, Kyoto, Japan), respectively. Gel imaging was carried out with a Bio-Rad imaging system. Transmission electron microscopic (TEM) and scanning electron microscopic (SEM) images were obtained with a JEM-2100 transmission electron microscope (JEOL, Ltd., Japan) and a Hitachi S4800 scanning electron microscope, respectively. X-ray powder diffraction

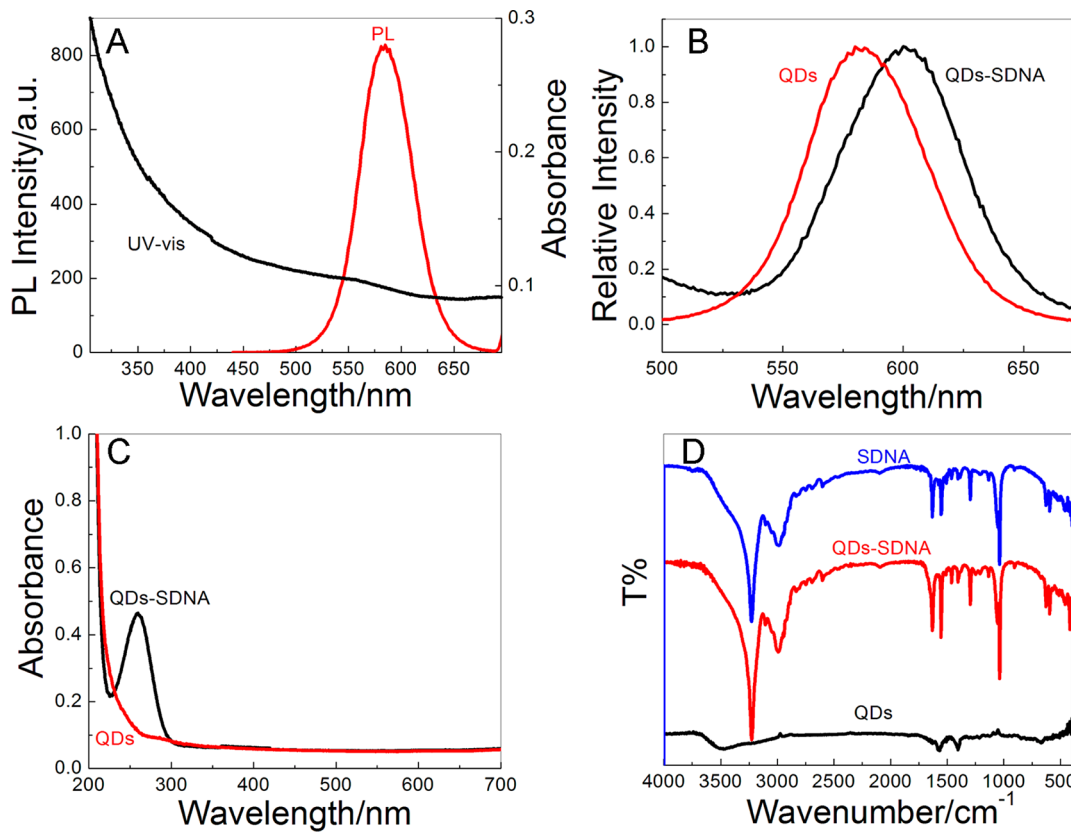


Figure 1. (A) Fluorescence and UV-vis absorption spectrum of QDs. (B) Normalized fluorescence spectra of QDs and QDs-SDNA. (C) UV-vis absorption spectra of QDs and QDs-SDNA. (D) FTIR spectra of QDs, SDNA, and QDs-SDNA.

(XRD) measurements were performed on a Japan Shimadzu XRD-6000 diffractometer with Cu K α radiation ($\lambda = 0.15418$ nm); a scanning rate of $0.05^\circ \text{ s}^{-1}$ was applied to record patterns in the 2θ range of 10 – 70° . Fourier-transform infrared (FTIR) spectroscopy was performed on a Bruker model VECTORT22 Fourier-transform spectrometer using KBr pressed disks. Static water contact angles were measured by a contact angle meter (Rame-Hart-100) employing drops of ultrapure water. Confocal scanning microscopy studies were performed on a Leica TCS SP5 microscope (Germany) with excitation at 405 nm. Electrochemical measurements were performed on a CHI 660B workstation (Shanghai Chenhua Apparatus Corporation, China) with a conventional three-electrode system composed of a platinum wire as the auxiliary, a saturated calomel electrode as the reference, and a mercury film modified glassy carbon electrode (GCE) as the working electrode. Electrochemical impedance spectroscopy (EIS) was performed with an Autolab electrochemical analyzer (Eco Chemie, The Netherlands) in 10 mM $\text{K}_3\text{Fe}(\text{CN})_6/\text{K}_4\text{Fe}(\text{CN})_6$ (1.0 M KCl) as the supporting electrolyte, within the frequency range of 0.01 to 100 kHz. Melting temperature (T_m) and the secondary structure of DNA were analyzed using OligoAnalyzer 3.1 (free online software from IDT).

Synthesis of SDNA-QDs and CDNA2-QDs Conjugates. CdTe QDs were synthesized according to literature procedures.^{13–15} The coupling reactions for SDNA and CDNA2 with QDs adopted the EDC/NHS method to form amides between the carboxyl groups of QDs and the primary amine groups of SDNA or CDNA2. Detailed procedures are included in the Supporting Information.

Preparation of Aptamer-DNA Concatamer-QDs. 1 μM CDNA1 was hybridized with 100 nM SDNA-QDs and 100 nM ADNA for 1 h in Tris buffer (pH 7.4) with the presence of 5 μM TCEP. The mixture was then subjected to ultrafiltration using a 100 kDa MW filter. After the lower phase was removed, the upper phase containing aptamer-DNA concatamer-QDs was decanted and stored at 4°C .

Construction of MWCNTs@PDA@AuNPs Composites. The MWCNTs@PDA were synthesized according to literature procedures.²⁷ Then, the MWCNTs@PDA were dispersed in HAuCl_4 solution. After that, aqueous sodium citrate was added into the above mixture drop by drop and stirred to get MWCNTs@PDA@AuNPs composites. More information about the protocol is described in the Supporting Information.

Cell Culture. CCRF-CEM and Ramos cells were cultured in a flask with a RPMI 1640 medium (Gibco, Grand Island, NY) supplemented with 10% fetal calf serum, penicillin (100 $\mu\text{g mL}^{-1}$), and streptomycin (100 $\mu\text{g mL}^{-1}$) in an incubator (5% CO_2 , 37°C). The density of cells was calculated using a Petroff-Hausser cell counter. After the concentration of cells reached 5×10^6 cells mL^{-1} , the cells were collected using centrifugation at 1000g for 3 min.

Fabrication of the Supersandwich Cytosensor. Prior to surface modification, the GCE ($d = 3$ mm) was polished with 0.05 mm alumina followed by successive sonication in acetone, HNO_3 (1:1 v/v), and distilled water, respectively. Afterward, 10 μL of MWCNTs@PDA@AuNPs solution was dropped onto GCE and dried to fabricate a functional film (GCE/MWCNTs@PDA@AuNPs). Then, 10 μL of Con A solution was dropped to the film and incubated at 4°C for 24 h. Following a rinse with buffer, the suspension of CCRF-CEM

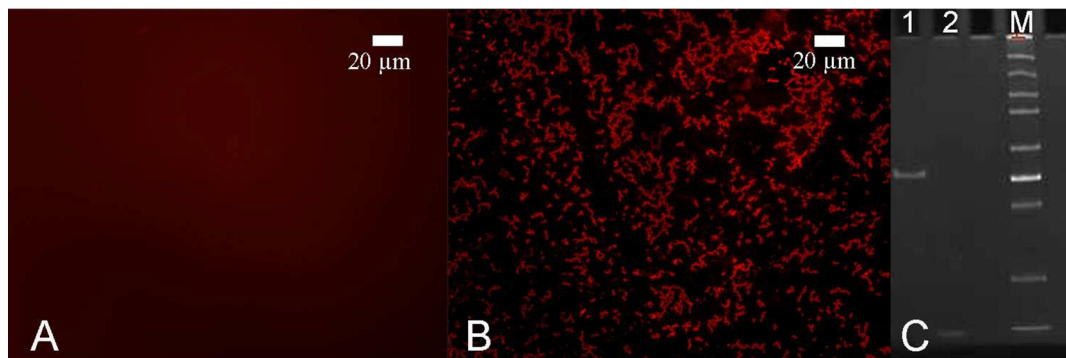


Figure 2. Fluorescence microscopy images of QDs (A) and aptamer-DNA concatamer-QDs (B). (C) The gel electrophoresis of aptamer-DNA concatamer-QDs. (lane 1, aptamer-DNA concatamer-QDs; lane 2, SDNA; lane M, DNA marker).

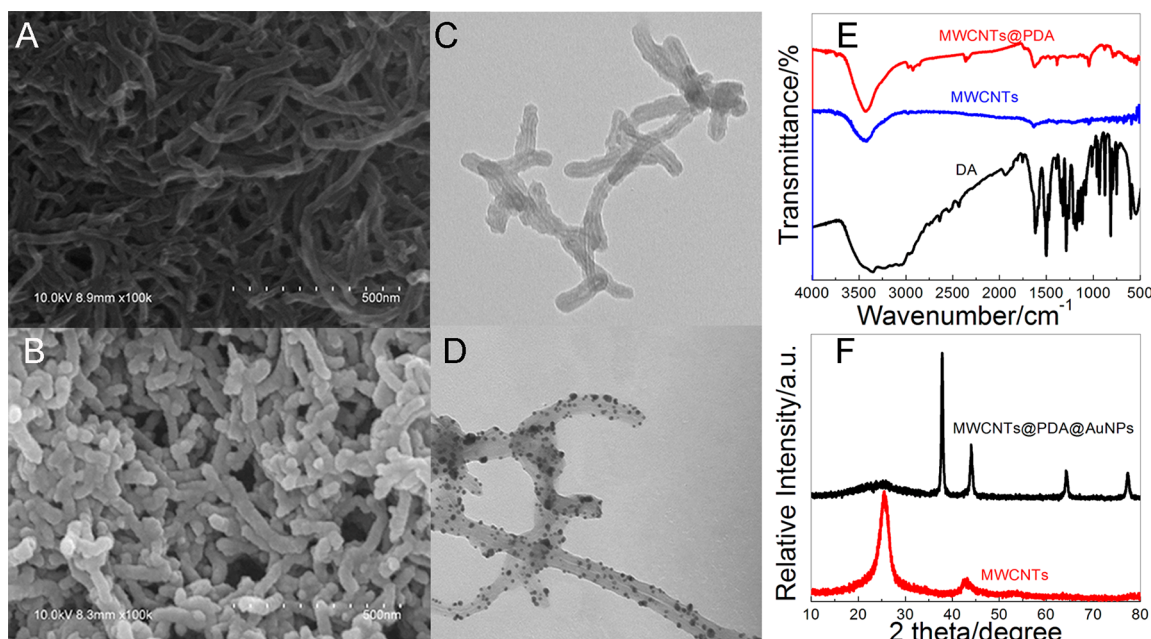


Figure 3. Representative SEM images of MWCNTs (A) and MWCNTs@PDA (B). TEM images of MWCNTs@PDA (C) and MWCNTs@PDA@AuNPs (D). (E) FTIR spectra of DA, MWCNTs, and MWCNTs@PDA. (F) XRD patterns of MWCNTs and MWCNTs@PDA@AuNPs.

cells ($20 \mu\text{L}$) at a certain concentration was dropped onto the GCE/MWCNTs@PDA@AuNPs/Con A film and incubated at 37°C for 2 h. After carefully washing with the buffer to remove noncaptured cells, $5 \mu\text{L}$ of aptamer-DNA concatamer-QDs was dropped onto the GCE/MWCNTs@PDA@AuNPs/Con A/cells film and incubated at 37°C for 1.5 h.

Electrochemical and Fluorescence Analysis. After the aptamer was bound to the GCE/MWCNTs@PDA@AuNPs/Con A/cells, the electrode was rinsed with buffer and immersed into HNO_3 ($200 \mu\text{L}$, 0.1 M) for 2 h to dissolve the residual QDs. Then, the concentrations of cells were determined with electrochemical and fluorescence methods (Supporting Information).

Confocal Microscopy Imaging. CCRF-CEM cells ($1 \times 10^5 \text{ cells mL}^{-1}$) were seeded onto a well plate. After 24 h, cells were incubated with aptamer-DNA concatamer-QDs probes for 1.5 h. To remove the unbound probes, the cells were washed three times with PBS. Then, the well was placed above a $20\times$ objective on the confocal microscope. QDs-aptamer was treated with the same procedures as the control experiment.

RESULTS AND DISCUSSION

Characterization of the QDs-SDNA. UV-vis, fluorescence, and FTIR spectroscopy were used to confirm the binding function between SDNA and QDs. In Figure 1A, QDs show an absorption peak at 550 nm and a strong fluorescence emission at 580 nm ($\lambda_{\text{ex}} = 350 \text{ nm}$). After SDNA was attached to QDs, an obvious absorption peak occurs at 260 nm as shown in Figure 1C, which is a characteristic of the DNA strand, indicating the successful binding between SDNA and QDs. In the case of fluorescence emission, both QDs and QDs-SDNA have symmetric Gaussian spectra, even though a slight red shift of the maximum emission wavelength from 580 to 600 nm is observed after SDNA functionalization (Figure 1B). The red shift can be ascribed to the increase of QDs' size.³⁷ The shape of the emission peak is almost the same before and after the modification of QDs with SDNA, suggesting well stability of covalent conjugation between QDs and SDNA. Furthermore, FTIR was also used to confirm the conjugation of SDNA and QDs. In Figure 1D, the peaks at 1590 and 3410 cm^{-1} correspond to the stretching vibrations of $\text{C}=\text{O}$ and $-\text{OH}$, respectively, which demonstrate the carboxylic group capping

on QDs. Compared with QDs, the characteristic absorption peaks of DNA at 1650, 1080, and 980 cm^{-1} are preserved after the formation of QDs-SDNA conjugates, which further prove the successful connection.

Characterization of Aptamer-DNA Concatamer-QDs.

To confirm the efficiency of aptamer-DNA concatamer-QDs replication, gel electrophoresis was used to verify the formation of a superstructure. In Figure 2C, aptamer-DNA concatamer-QDs produce one band at 750–1000 bp, while SDNA has one band at less than 75 bp. The results show that aptamer-DNA concatamer-QDs have long DNA strands, and the hybridization reaction is implemented by SDNA, CDNA1, and ADNA. Therefore, the reaction of DNA concatamers can be triggered and progressed with the guidance of the CDNA1 primers between SDNA and ADNA. According to the base pairs in one unit, the number of signal centers incorporated into single superstructure is 25. Furthermore, the formation of aptamer-DNA concatamer-QDs is also observed by fluorescence microscopy images, as shown in Figure 2A and B. No obvious shape appears in Figure 2A, while a DNA wire containing a large number of QDs is displayed as a regularly aggregated state with a length up to micrometer scale (Figure 2B), which is comparable with previous works.^{38,39} The phenomenon is attributed to the hybridization of QDs-SDNA to the corresponding ADNA and CDNA1, which indicates that the micrometer-dimension, wire-like morphology is DNA-based material and also confirms the successful assembly of the supramolecular aptamer-DNA concatamer-QDs.

Characterization of MWCNTs@PDA@AuNPs Composites.

Inspired by mussel-adhesion phenomena in nature, MWCNTs@PDA@AuNPs were fabricated by PDA as interlinkers. First, MWCNTs were dispersed in DA solution for 24 h. Then, AuNPs were deposited on the PDA layer by stirring MWCNTs@PDA with HAuCl₄ solution in the presence of sodium citrate. After that, the morphology and size of the above composites were characterized by TEM and SEM. Compared with MWCNTs (Figure 3A), the surface of MWCNTs@PDA becomes rough and fatter (Figure 3B), which indicates that MWCNTs have been coated with PDA. The interface of the MWCNTs sidewall and PDA is clearly observed as shown in Figure 3C. All of the MWCNTs are wrapped by polymer shells with a lighter color than MWCNTs. After treatment by HAuCl₄, dark particles of 5 nm are observed to be adhered individually on nanotubes (Figure 3D). Furthermore, FTIR spectroscopy was used to evaluate the surface functionalization by PDA and AuNPs. In Figure 3E, DA as a feature of small molecule shows narrow peaks. The pure MWCNTs give weak absorption bands at 1615 and 3420 cm^{-1} , indicating a few carboxyl groups exist on the surface of MWCNTs. In contrast, MWCNTs@PDA show intense absorption features such as those of PDA due to the affinity between PDA aromatic rings and MWCNTs side walls.^{40,41} The XRD pattern was used to characterize the structure and phase of MWCNTs@PDA@AuNPs, as shown in Figure 3F. The intense reflection of MWCNTs is located at 26.4° (basal (002)). After MWCNTs were treated with HAuCl₄, the XRD pattern shows new reflection peaks at 38.2°, 44.4°, 64.5°, and 77.7°, corresponding to (111), (200), (220), and (311) crystallographic orientations of fcc Au, respectively.⁴² The new series of intense basal reflections indicates that AuNPs are successfully deposited on MWCNTs@PDA. The composites provide a platform to fix enough Con A due to the strong interaction between AuNPs and Con A.

Characterization of Con A-Based Biosensor. The hydrophilicity of the prepared materials was also studied using contact angle measurements. As shown in Figure S1A (Supporting Information), the contact angles of MWCNTs (a), MWCNTs@PDA (b), and MWCNTs@PDA@AuNPs films (c) were 41°, 25°, and 17°, respectively. Among them, MWCNTs@PDA@AuNPs show the lowest contact angle, indicating the best hydrophilicity, which may be attributed to the formation of AuNPs and PDA films. Therefore, MWCNTs@PDA@AuNPs can provide a biocompatible surface to enhance protein loading and retain bioactivity.

As an effective tool for probing interface features, EIS was used to study the stepwise assembly of the cytosensor.^{43,44} The impedance spectra include a semicircle portion and a linear portion. The semicircle portion at higher frequencies corresponds to the electron-transfer-limited process, and the linear portion at lower frequencies represents the diffusion-limited process. The semicircle diameter equals the electron-transfer resistance.⁴⁶ Figure S1B (Supporting Information) shows the nyquist plots of EIS upon the stepwise modification processes. At a bare GCE, the redox process of the probe displays an electron-transfer resistance of 475 Ω (curve a), while the MWCNTs@PDA@AuNPs modified electrode has a lower resistance for the redox probe (curve b), demonstrating an excellent conducting material for accelerating electron transfer. After immersing into Con A solution, the resistance increases to 1280 Ω (curve c), which suggestss that Con A was immobilized on the electrode and blocked electron transfer between the redox probe and electrode. After capture of the cells, the resistance increases again (curve d) due to the dielectric behavior of cells for the interfacial electron-transfer process. Additionally, the access of the redox probe to the electrode was further hindered after incubation with aptamer-DNA concatamer-QDs probes because of the resistance of DNA (curve e). These results indicate the successful fabrication of the supersandwich cytosensor. Furthermore, Calcein-AM staining experiments were selected to characterize the MWCNTs@PDA@AuNPs/Con A film for the catch of target cells. As shown in Figure S2 (Supporting Information), strong fluorescence was observed after the MWCNTs@PDA@AuNPs/Con A film incubated with target cells, indicating a large number of viable cells were effectively captured by the MWCNTs@PDA@AuNPs/Con A. Thus, the MWCNTs@PDA@AuNPs/Con A-modified interface could capture the target cells with high efficiency and maintain cells that are live.

Optimization of Experimental Conditions. Electrochemical performance of the cytosensor is influenced by some parameters such as the concentration of MWCNTs@PDA@AuNPs and Con A, the time of specific recognition between aptamer and cells, and the pH of the buffer. To improve the sensitivity, the concentration of MWCNTs@PDA@AuNPs was optimized first. As shown in Figure S3A (Supporting Information), a significant increase of the peak current is observed between 0.5 and 4.0 mg mL^{-1} . Further increasing the concentration of material from 4.0 to 8.0 mg mL^{-1} did not significantly improve the electrochemical signal. Therefore, 4.0 mg mL^{-1} of MWCNTs@PDA@AuNPs was selected as the optimal concentration in the electrode modification. In addition, the effect of Con A concentration on the peak current was investigated. The highest current is achieved at 4 mg mL^{-1} among different Con A concentrations (0.01–6 mg mL^{-1} ; Figure S3B, Supporting Information). At low concentrations of Con A (<4 mg mL^{-1}), the binding of

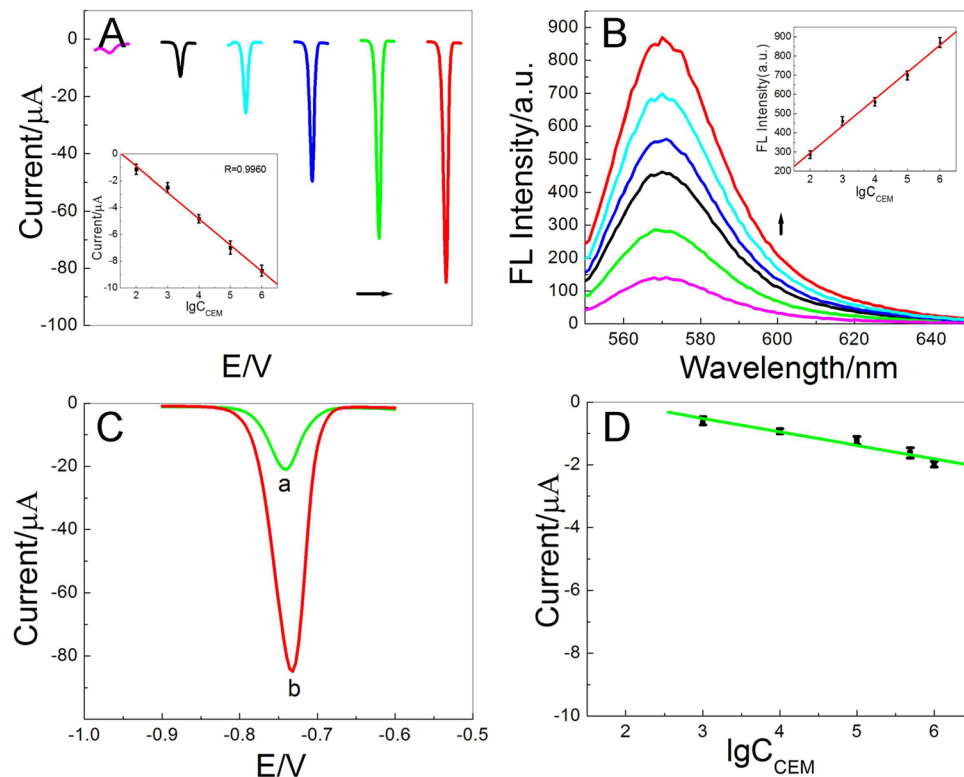


Figure 4. (A) Anodic stripping voltammetric (ASV) of the supersandwich cytosensor incubated with different concentrations of CCRF-CEM cells: 0, 10², 10³, 10⁴, 10⁵, and 10⁶ cells mL⁻¹ (left to right). Inset: the corresponding linear calibration plots. (B) Fluorescence spectra of Rhod-SN responding for different concentrations of CCRF-CEM cells: 0, 10², 10³, 10⁴, 10⁵, and 10⁶ cells mL⁻¹ (down to up). Inset: the corresponding linear calibration plots. (C) ASV of the modified electrode in 10⁶ cells mL⁻¹ cancer cells after being incubated with conventional sandwich (a) and supersandwich structure (b). (D) Calibration plots of current vs logarithm of CCRF-CEM cancer cell concentration in the presence of the QDs-aptamer probes.

Con A with cells is insufficient; while at high concentrations (>4 mg mL⁻¹), the binding is saturated. Therefore, 4 mg mL⁻¹ was chosen as the optimized concentration. Furthermore, recognition time is an important parameter for the kinetic binding between aptamer and cells. Figure S3C (Supporting Information) shows the relationship between recognition time and peak current. The current elevates with increasing incubation time and starts to level off after 1.5 h. Thus, 1.5 h was selected as the best recognition time. The effect of pH was also discussed. The electrochemical response of pH ranging from 4.4 to 5.4 is shown in Figure S3D (Supporting Information). The highest signal was obtained at pH 5.2, and this pH value was selected in the following experiments.

Electrochemical Detection of Cancer Cells. For the detection of cancer cells, high sensitivity and selectivity play an important role in improving treatment. In view of this, the proposed supersandwich cytosensor was applied to quantify cancer cells. Figure 4A shows the linear calibration plots of the peak current (Δi_p) versus the concentration of CCRF-CEM cells. A linear relationship between Δi_p and the logarithm of the cell concentration is found in the range of 1.0×10^2 to 1.0×10^6 cells mL⁻¹. The linear regression equation is Δi_p (μ A) = $3.00 - 1.96 \lg C_{\text{cells}}$ (cells mL⁻¹) with a correlation coefficient of 0.9960 ($n = 3$). The detection limit is estimated to be 50 cells mL⁻¹ at 3σ .

In order to explain the enhanced sensitivity of the supersandwich strategy, QDs-aptamer was compared with aptamer-DNA concatamer-QDs as the control. Although the peak current rises with the increase of cell concentrations

(Figure 4D), the slope of the plots for peak current vs logarithmic cell concentrations using QDs-aptamer is about 5.6 times lower than that of aptamer-DNA concatamer-QDs. In addition, the detection limit of the conventional sandwich based on QDs-aptamer probes is higher than that of the supersandwich assay. The results show that the enhanced sensitivity comes from the signal amplification of the aptamer-DNA concatamer-QDs probes.

Fluorescence Detection of Cancer Cells. Considering the outstanding signal amplification of Rhod-SN dye by Cd²⁺, the dynamic range for detecting CCRF-CEM cells with the fluorescence method was also examined. The fluorescence intensity of Rhod-SN dye elevates upon increasing the concentration of CCRF-CEM cells (Figure 4B). A good linear relationship between the fluorescence intensity and logarithm of cell concentrations is obtained in the range of 10^2 to 10^6 cells mL⁻¹. The detection limit is 50 cells mL⁻¹ at 3σ , which is lower than that of 6000 cells mL⁻¹ with an EIS cytosensor⁴⁵ or 8000 cells mL⁻¹ with a quartz crystal microbalance (QCM) cytosensor.⁴⁶

Performance of the Supersandwich Cytosensor. Good selectivity is required for the detection of leukemia patients. To assess the specificity of the supersandwich strategy toward CCRF-CEM cells, Ramos cells were used as the control. In this work, the specificity was evaluated by testing the response of the assay in the presence of CCRF-CEM cells or Ramos cells at a concentration of 1.0×10^6 cells mL⁻¹. The peak current of the cytosensor negligibly changed with the addition of the control cells (8.691 μ A), while a significant electrochemical

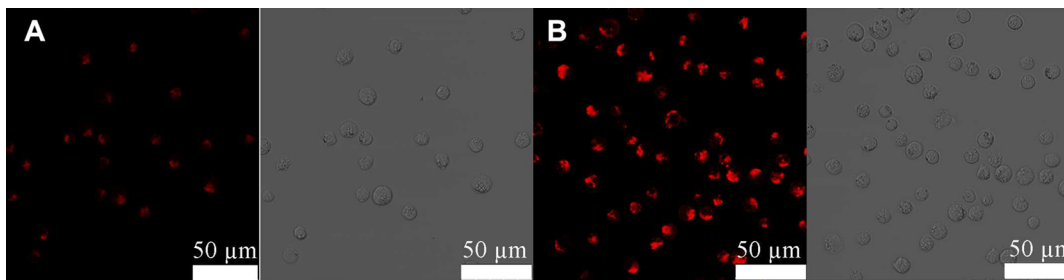


Figure 5. Confocal microscopy images of CCRF-CEM cells stained by QDs-aptamer (A) and aptamer-DNA concatamer-QDs (B) probes, scale bar: 50 μm .

signal increase was observed for CCRF-CEM cells ($83.75 \mu\text{A}$). The results also show that the signal of Ramos cells incubated with aptamer-DNA concatamer-QDs probes is similar to that of only probes incubated with the electrode, which demonstrates a good specificity for CCRF-CEM cells using the proposed strategy. Taking various kinds of aptamers for cells into account, the proposed method can be applied for the specific detection of CCRF-CEM cells and other kinds of cancer cells if appropriate aptamers are selected.

At a concentration of 1.0×10^5 cells mL^{-1} , the proposed method shows relative standard deviations of 7.0% for electrochemical detection and 3.5% for fluorescence detection at three replicate measurements, respectively. The precision and reproducibility of the proposed method are acceptable. Moreover, the stability was also examined. When the cytosensor was stored at 4°C , the analytical performance did not decline obviously, showing a good stability. The stability is attributed to the stable structure of probes and the strong interaction between MWCNTs@PDA@AuNPs and Con A. Thus, the designed strategy shows good performance for the detection of cancer cells with a broad detection range, low detection limit, excellent selectivity, good reproducibility, and stability.

Furthermore, the analytical performance of the supersandwich cytosensor was compared with that of reported sensors. Characteristics such as linear range and detection limit are summarized in S-Table (Supporting Information). The supersandwich cytosensor shows attractive performance for the quantification of CCRF-CEM cells, such as a wide linear range and low detection limit. The reason may be as follows: first, MWCNTs provide large specific surface areas to promise abundant binding of AuNPs. Combining the excellent conductivity of MWCNTs with the extraordinary biocompatibility of AuNPs, the MWCNTs@PDA@AuNPs composites are very suitable for immobilizing Con A with high stability and bioactivity. It provides an ideal interface for cell capture, therefore improving the sensitivity of detection. Second, the supersandwich strategy further enhances the sensitivity *via* the signal amplification of aptamer-DNA concatamer-QDs. The introduction of an aptamer-DNA concatamer-QDs probe leads to a remarkable increase of the signal.

Confocal Microscopy Imaging. The specific binding between aptamer and target cells and the signal amplification of the aptamer-DNA concatamer-QDs probes were also studied by confocal microscopy imaging. In order to show the specific binding of aptamer-DNA concatamer-QDs with the target cells, aptamer-DNA concatamer-QDs were incubated with CCRF-CEM cells at 37°C . As shown in Figure 5B, the extracellular aptamer-DNA concatamer-QDs provide strong fluorescence, which suggests that the probes can effectively bind CCRF-CEM

cells. To further prove the signal amplification effect of the aptamer-DNA concatamer-QDs, a control experiment was carried out by staining CCRF-CEM cells with QDs-aptamer. Figure 5A shows much lower fluorescence intensity of QDs-aptamer than that of aptamer-DNA concatamer-QDs after the same exposure time. The reason is that the latter probe contains dozens of QDs, whereas the former one contains only one QD.

CONCLUSIONS

A versatile supersandwich cytosensor has been developed by combining the technique of DNA concatamer amplification, the specific binding of aptamer and the optical and electrical properties of QDs, with the fluorescence and electrochemical methods. In the fabrication of the supersandwich cytosensor, MWCNTs@PDA@AuNPs composites were used to load a large amount of Con A for the specific recognition of cells and enhance the sensitivity of detection. Furthermore, aptamer-DNA concatamer-QDs as the fluorescence and electrochemical probes were used to specifically bind CCRF-CEM cells and increase the sensitivity dramatically. The proposed supersandwich cytosensor shows excellent sensitivity and selectivity, wide linear range, good reproducibility, acceptable precision, and accuracy. In view of these advantages, this supersandwich cytosensor has great potential in the field of disease diagnostics and clinical analysis.

ASSOCIATED CONTENT

Supporting Information

Additional experimental procedures, supplemental figures, and a supplemental table. This material is available free of charge via the Internet at <http://pubs.acs.org>.

AUTHOR INFORMATION

Corresponding Authors

*Phone and Fax: +86-25-83597204. E-mail: jjzhu@nju.edu.cn; Phone and Fax: +86-25-83597204. E-mail: denganping@suda.edu.cn.

Author Contributions

H.L. and S.X. contributed equally to this work.

Notes

The authors declare no competing financial interest.

ACKNOWLEDGMENTS

This work was supported by National Basic Research Program of China (2011CB933502). We greatly appreciate the support of National Natural Science Foundation of China (No. 21121091, No. 21175097) and Postdoctoral Science Foundation of China (No. 2012M511236).

■ REFERENCES

- (1) Nagrath, S.; Sequist, L. V.; Maheswaran, S.; Bell, D. W.; Irimia, D.; Ulkus, L.; Smith, M. R.; Kwak, E. L.; Digumarthy, S.; Muzikansky, A.; Ryan, P.; Balis, U. J.; Tompkins, R. G.; Haber, D. A.; Toner, M. *Nature* **2007**, *450*, 1235–1239.
- (2) Galanzha, E. I.; Shashkov, E. V.; Kelly, T.; Kim, J. W.; Yang, L.; Zharov, V. P. *Nat. Nanotechnol.* **2009**, *4*, 855–860.
- (3) Xu, Y.; Phillips, J. A.; Yan, J.; Li, Q.; Fan, Z. H.; Tan, W. *Anal. Chem.* **2009**, *81*, 7436–7442.
- (4) Singh, S. K.; Hawkins, C.; Clarke, I. D.; Squire, J. A.; Bayani, J.; Hide, T.; Henkelman, R. M.; Cusimano, M. D.; Dirks, P. B. *Nature* **2004**, *432*, 396–401.
- (5) Schamhart, D.; Swinnen, J.; Kurth, K. H.; Westerhof, A.; Kuster, R.; Borchers, H.; Sternberg, C. *Clin. Chem.* **2003**, *49*, 1458–1466.
- (6) Phillips, J. A.; Xu, Y.; Xia, Z.; Fan, Z. H.; Tan, W. H. *Anal. Chem.* **2009**, *81*, 1033–1039.
- (7) López-Colón, D.; Jiménez, E.; You, M.; Gulbakan, B.; Tan, W. *WIREs Nanomed. Nanobiol.* **2011**, *3*, 328–340.
- (8) Shangguan, D.; Li, Y.; Tang, Z.; Cao, Z. C.; Chen, H. W.; Mallikaratchy, P.; Sefah, K.; Yang, C. J.; Tan, W. *Proc. Natl. Acad. Sci. U. S. A.* **2006**, *103*, 11838–11843.
- (9) Bagalkot, V.; Farokhzad, O. C.; Langer, R.; Jon, S. *Angew. Chem., Int. Ed.* **2006**, *45*, 8149–8152.
- (10) Huang, Y. F.; Chang, H. T.; Tan, W. H. *Anal. Chem.* **2008**, *80*, 567–572.
- (11) Sun, Z. P.; Wang, Y. L.; Wei, Y. T.; Liu, R.; Zhu, H. R.; Cui, Y.; Zhao, Y. L.; Gao, X. Y. *Chem. Commun.* **2011**, *47*, 11960–11962.
- (12) Zhang, J. J.; Zheng, T. T.; Cheng, F. F.; Zhang, J. R.; Zhu, J. J. *Anal. Chem.* **2011**, *83*, 7902–7909.
- (13) Qian, H. F.; Dong, C. Q.; Weng, J. F.; Ren, J. C. *Small* **2006**, *2*, 747–751.
- (14) Zhang, H.; Wang, D.; Yang, B.; Mohwald, H. *J. Am. Chem. Soc.* **2006**, *128*, 10171–10180.
- (15) Cui, R. J.; Pan, H. C.; Zhu, J. J.; Chen, H. Y. *Anal. Chem.* **2009**, *79*, 8494–8501.
- (16) Liu, G. D.; Wang, J.; Kim, J.; Jan, M. R. *Anal. Chem.* **2004**, *76*, 7126–7130.
- (17) Gill, R.; Zayats, M.; Willner, I. *Angew. Chem., Int. Ed.* **2008**, *47*, 7602–7625.
- (18) Li, J. S.; Zhang, T. R.; Ge, J. P.; Yin, Y. D.; Zhong, W. W. *Angew. Chem., Int. Ed.* **2009**, *48*, 1588–1591.
- (19) Li, J. S.; Schachermeyer, S.; Wang, Y.; Yin, Y. D.; Zhong, W. W. *Anal. Chem.* **2009**, *81*, 9723–9729.
- (20) Sheng, Z. H.; Hu, D. H.; Zhang, P. F.; Gong, P.; Gao, D. Y.; Liu, S. H.; Cai, L. T. *Chem. Commun.* **2012**, *48*, 4202–4204.
- (21) Han, E.; Ding, L.; Ju, H. X. *Anal. Chem.* **2011**, *83*, 7006–7012.
- (22) Trojanowicz, M. *Trends Anal. Chem.* **2006**, *25*, 480–489.
- (23) Caruso, F. *Top Curr. Chem.* **2003**, *227*, 145–168.
- (24) El-Said, W. A.; Kim, T. H.; Kim, H.; Choi, J. W. *Biosens. Bioelectron.* **2010**, *26*, 1486–1492.
- (25) Xu, W.; Xue, X. J.; Li, T. H.; Zeng, H. Q.; Liu, X. G. *Angew. Chem., Int. Ed.* **2009**, *48*, 6849–6852.
- (26) Lee, H.; Dellatore, S. M.; Miller, W. M.; Messersmith, P. B. *Science* **2007**, *318*, 426–430.
- (27) Fei, B.; Qian, B.; Yang, Z.; Wang, R.; Liu, W. C.; Mak, C. L.; Xin, J. H. *Carbon* **2008**, *46*, 1795–1797.
- (28) Cao, Y. C.; Jin, R.; Mirkin, C. A. *Science* **2002**, *297*, 1536–1540.
- (29) Zuo, X. L.; Xiao, Y.; Plaxco, K. W. *J. Am. Chem. Soc.* **2009**, *131*, 6944–6945.
- (30) Lin, Z. Y.; Chen, L. F.; Zhu, X.; Qiu, B.; Chen, G. N. *Chem. Commun.* **2010**, *46*, 5563–5565.
- (31) Zhang, X. A.; Teng, Y. Q.; Fu, Y.; Zhang, S. P.; Wang, T.; Wang, C. G.; Jin, L. T.; Zhang, W. *Chem. Sci.* **2011**, *2*, 2353–2360.
- (32) Xia, F.; White, R. J.; Zuo, X. L.; Patterson, A.; Xiao, Y.; Kang, D.; Gong, X.; Plaxco, K. W.; Heeger, A. J. *J. Am. Chem. Soc.* **2010**, *132*, 14346–14348.
- (33) Wang, G. F.; Huang, H.; Wang, B. J.; Zhang, X. J.; Wang, L. *Chem. Commun.* **2012**, *48*, 720–722.
- (34) Yin, B. C.; Guan, Y. M.; Ye, B. C. *Chem. Commun.* **2012**, *48*, 4208–4210.
- (35) Chen, X.; Lin, Y. H.; Li, J.; Lin, L. S.; Chen, G. N.; Yang, H. H. *Chem. Commun.* **2011**, *47*, 12116–12118.
- (36) Yuan, T.; Liu, Z. Y.; Hu, L. Z.; Zhang, L.; Xu, G. B. *Chem. Commun.* **2011**, *47*, 11951–11953.
- (37) Li, Y. Q.; Wang, J. H.; Zhang, H. L.; Yang, J.; Guan, L. Y.; Chen, H.; Luo, Q. M.; Zhao, Y. D. *Biosens. Bioelectron.* **2010**, *25*, 1283–1289.
- (38) Deng, Z. X.; Tian, Y.; Lee, S. H.; Ribbe, A. E.; Mao, C. D. *Angew. Chem., Int. Ed.* **2005**, *44*, 3582–3585.
- (39) Tong, P.; Zhao, W. W.; Zhang, L.; Xu, J. J.; Chen, H. Y. *Biosens. Bioelectron.* **2012**, *33*, 146–151.
- (40) Fei, B.; Qian, B.; Yang, Z.; Wang, R.; Liu, W. C.; Mak, C. L.; Xin, J. H. *Carbon* **2008**, *46*, 1795–1797.
- (41) Wang, G. F.; Huang, H.; Zhang, G.; Zhang, X. J.; Fang, B.; Wang, L. *Langmuir* **2011**, *27*, 1224–1231.
- (42) Lee, K. Y.; Lee, Y. W.; Kwon, K.; Heo, J.; Kim, J.; Han, S. W. *Chem. Phys. Lett.* **2008**, *453*, 77–81.
- (43) Li, X. H.; Dai, L.; Liu, Y.; Chen, X. J.; Yan, W.; Jiang, L. P.; Zhu, J. J. *Adv. Funct. Mater.* **2009**, *19*, 3120–3128.
- (44) Chen, X. J.; Wang, Y. Y.; Zhou, J. J.; Wei, Y.; Li, X. H.; Zhu, J. J. *Anal. Chem.* **2008**, *80*, 2133–2140.
- (45) Pan, C. F.; Guo, M. L.; Nie, Z.; Xiao, X. L.; Yao, S. Z. *Electroanalysis* **2009**, *21*, 1321–1326.
- (46) Pan, Y. L.; Guo, M. L.; Nie, Z.; Huang, Y.; Pan, C. F.; Zeng, K.; Zhang, Y.; Yao, S. Z. *Biosens. Bioelectron.* **2010**, *25*, 1609–1614.